Validated numerics for continuation and bifurcation of connecting orbits of maps

Ronald Adams *[1] and J.D. Mireles James †[2]

[1]Embry-Riddle Aeronautical University, Department of Mathematics
[2]Florida Atlantic University, Department of Mathematical Sciences

July 19, 2017

Abstract

Validated numerical computations are used to study one parameter branches of connecting orbits and their bifurcations. The idea is to formulate the connecting orbit as a zero of a certian finite dimensional map. Computer assisted methods of proof for continuation and bifurcation of zeros are applied to the map, providing global results for the underlying dynamical system. We use the parameterization method to represent the local stable/unstable manifolds of the fixed point, and focus on the example of the Hénon map.

1 Introduction

This paper describes self validating numerical algorithms for mathematically rigorous computation of smooth branches of connecting orbits, and bifurcations of these branches. We focus on discrete time dynamical systems with a single parameter. More precisely, let $f\colon \mathbb{R}^n \times \mathbb{R} \to \mathbb{R}^n$ be a one parameter family of diffeomorphisms and suppose that for some fixed $\lambda_1 \in \mathbb{R}$ there is a hyperbolic fixed point $\hat{p} \in \mathbb{R}^n$, i.e. that

$$f(\hat{p}, \lambda_1) = \hat{p},$$

and that $Df(\hat{p}, \lambda_1)$ (which is an invertible matrix as f is a diffeomorphism) has no eigenvalues on the unit circle. Then, by the implicit function theorem, there is a $\epsilon > 0$ and a smooth function $p\colon (\lambda_1 - \epsilon, \lambda_1 + \epsilon) \to \mathbb{R}^n$ so that $p(\lambda_1) = \hat{p}$ and

$$f(p(\lambda)) = p(\lambda),$$

*R.A. partially supported by NSF grant DMS - 1318172 Email: ADAMSR25@erau.edu

†J.M.J partially supported by NSF grant DMS - 1318172 and by the Alfred P. Sloan Foundation grant G-2016-7320. Email: jmirelesjames@fau.edu

for all $\lambda \in (\lambda_1 - \epsilon, \lambda_1 + \epsilon)$. Moreover, ϵ can be chosen small enough so that $Df(p(\lambda), \lambda)$ is hyperbolic for all $\lambda \in (\lambda_1 - \epsilon, \lambda_1 + \epsilon)$. Hyperbolicity for each such λ guarantees that there are stable and unstable manifolds attached to the $p(\lambda)$, and that the sum of their dimensions equals the dimension of the phase space. We denote this one parameter family of manifolds by $W^s(\lambda)$ and $W^u(\lambda)$, suppressing the dependance on $p(\lambda)$ and $f(\cdot, \lambda)$. Recall that the manifolds depend smoothly on λ.

Once again fixing $\lambda = \lambda_1$, we say that a point $x_1 \in \mathbb{R}^n$ is *homoclinic* for the fixed point $\hat{p}$ under the map $f(\cdot, \lambda_1)$ if

$$\lim_{n \to \pm\infty} f^n(x_1, \lambda_1) = \hat{p}.$$

Note that a homoclinic point x_1 must, by definition, lie in the intersection of the stable and unstable manifolds of p_1: i.e.

$$x_1 \in W^s(\lambda_1) \cap W^u(\lambda_1).$$

We say that x_1 is a transverse homoclinic point if

$$\text{span}\,(T_{x_1} W^s(\lambda_1), T_{x_1} W^u(\lambda_1)) = \mathbb{R}^n,$$

i.e. if the stable and unstable manifolds of $\hat{p}$ intersect transversally at x_1.

Since the manifolds vary smoothly in λ, and since transverse intersections are robust, we can take $\epsilon > 0$ so small that there is a transverse intersection point for each $\lambda \in (\lambda_1 - \epsilon, \lambda_1 + \epsilon)$. More precisely, there is a smooth function $x_1 \colon (\lambda_1 - \epsilon, \lambda_1 + \epsilon) \to \mathbb{R}^n$ having that $x(\lambda_1) = x_1$ and that

$$x_1(\lambda) \in W^s(\lambda) \cap W^u(\lambda),$$

for all $\lambda \in (\lambda_1 - \epsilon, \lambda_1 + \epsilon)$. The situation is depicted pictorially in Figure 1.

Note that a smooth branch of connecting orbits continues until (a) - the transversality assumption breaks down, or (b) the hyperbolicity of the fixed point is lost. Restricting to co-dimension one bifurcations of type (a), we see that a loss of transversality occurs when two connecting orbits collide and disappear as illustrated in Figure 1, i.e. when manifold intersections are born or when they vanish. In the language of catastrophe theory we have that case (a) corresponds to a saddle-node bifurcation of the branch $x(\lambda)$ – which in this setting is a branch of connecting orbits. Consideration of case (b) is more delicate, as the loss of hyperbolicity introduces center manifold theory into the conversation. We postpone further discussion of case (b) to a future study.

In the remainder of the paper we focus on developing computational techniques for mathematically rigorous study of smooth branches of connecting orbits, and their bifurcations as just discussed. Our methods are designed so that, in addition to proving abstract existence results, we obtain validated numerical bounds on the distance between the true and approximate connections. The following developments guide our approach.

The method of projected boundaries – connecting orbit as a zero of a higher dimensional operator: we first reformulate the connecting orbit as an

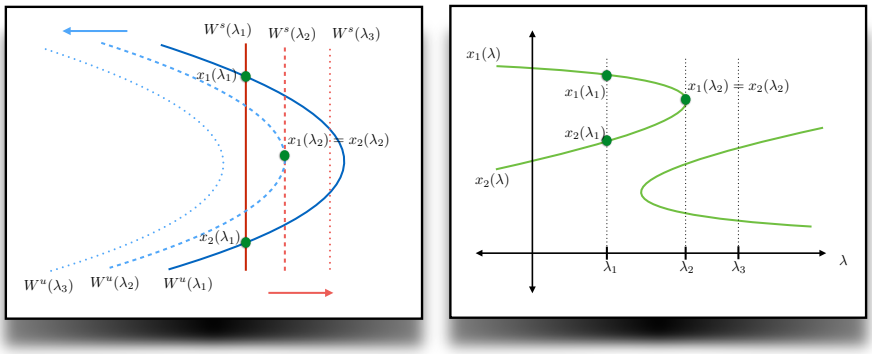

Figure 1: Left: transverse intersection of the stable/unstable manifolds giving rise to a family of connecting orbits. As the parameter changes the intersection moves closer to a tangency, at which point the intersection is broken. Right: the associated fold bifurcation for the homoclinic point.

isolated zero of a certain nonlinear funciotn, which we call the *connecting orbit operator* (see Section 3 for the precise formulation of this notion). The idea is to think of the connecting orbit as the solution of a discrete time boundary value problem, with boundary conditions on the local stable/unstable manifolds. This classic approach is sometimes referred to as *the method of projected boundaries* [13, 7, 5, 6, 12, 11].

Validated numerics for the method of projected boundaries: *Validated numerics* refers to a whole suite of techniques in numerical analysis, which result in mathematically rigorous existence as well as tight error bounds between the true and approximate solution of the problem. Many such techniques are based on a-posteriori analysis, i.e. we first compute an approximate numerical solution of our problem and then we analyze the results. A successful validated numerical scheme involves choosing (or developing) an appropriate a-posteriori existence and uniqueness theorem (sometimes called a *constructive implicit function theorem* or a *Newton-Kantorovich theorem*), followed by careful hypothesis checking using – often using *interval arithmetic* to manage round off errors. Much more discussion, as well as more thorough review of the literature, is found in the review articles [24, 36, 34, 23], as well as the books [25, 35, 14].

Validated numerical methods based on the method of projected boundaries are developed in [31, 28], and provide computer assisted proofs for connecting orbits in discrete and continuous time dynamical systems. The main idea is to apply rigorous zero finding/enclosing schemes to the appropriate connecting

orbit operators. In addition to producing abstract existence and enclosure results, the methods of [31, 28] provide automatically the transversality of the connection.

Validated numerics for rigorous branch following: A number of authors have developed validated numerical methods for studying smooth branches of zeros. The studies most closely related to the present work include the references [10, 37, 4, 33, 38, 8]. The interested reader will find many additional references therein. We refer also the the Lecture notes [26].

Validated numerics for a saddle node bifurcation: There also exist validated numerical methods for studying bifurcations of solutions of operator equations. See for example the works of [33, 4, 27]. Our approach is adapted directly from the last of these references.

The techniques discussed above comprise the main ingredients in the present work. We exploit the formulation of connecting orbits as zeros of nonlinear operator equations, in concert with validated numerical methods for rigorous branch following, to prove the existence of smooth branches of connecting orbits with tight error bounds. Moreover, validated numerical techniques for saddle node bifurcation analysis allow us to study branches of connecting orbits from birth do death, at least in the case that the underlying fixed point itself undergoes no stability bifurcation.

Remark 1.1. The present study is closely related to the recent work of [8], which treats heteroclinic arcs arising from the transverse intersection of a k-dimensional unstable manifold and an m-dimensional stable manifold, where $k + m = n + 1$. Note that these intersection arcs occur in fixed dynamical systems, i.e. in contrast to the parameter dependent problems considered in the present work, no parameters are involved in the work of [8].

A more technical remark concerns the treatment of function compositions, which are notoriously problematic for interval arithmetics. The work of [8] exploits a Lohner type scheme based on coordinate frames adapted to the expanding and contracting directions of f along the connecting orbit. Such Lohner schemes are useful for mitigating the so called "wrapping effect" [29, 39].

In the present work we exploit a "multiple shooting" scheme which has been used successfully in recent studies to mitigate the wrapping effect [31, 18]. The idea is to introduce additional variables and solve an expanded system of equations which involves no compositions of the map f. This scheme minimizes the wrapping effect while avoiding the use of special coordinates, at the cost of increasing the dimension of the problem.

The present work builds also on the study of of [30], where the second author developed validated numerical methods for studying one parameter families of stable/unstable manifolds. The techniques developed in the reference just cited allow us to include the systems parameter in the connecting orbit operator.

We also mention the related work of [3, 2, 1], on existence and continuation of homoclinic tangencies in two parameter families of discrete time dynamical systems. The authors prove the existence of tangencies (i.e. a saddle node

bifurcation point for a branch of connecting orbits), and study the behavior of such points as the two parameters are varied. The authors use algebraic topological constructions based on the Conley index theory. However branches of transverse homoclinic points are not studied in the reference just cited.

1.1 Our main example

We implement our method for the particular example of the classical Hénon map

$$f(x,y) = \begin{pmatrix} 1 + y - \lambda x^2 \\ bx \end{pmatrix}, \tag{1}$$

with $b = 0.3$. The simple form of the map eases the presentation of the technical material to follow. We consider the system with λ the parameter.

The dynamics as a function of λ are illustrated in the four frames of Figure 2, and also in Figure 5. In particular, the images illustrate the fact that homoclinic intersection points are prevalent in the Hénon system.

2 The parameterization method

The parameterization method is a general functional analytic framework for studying invariant manifolds. For a high level introduction to the method, we refer to the series of papers [15, 16, 17, 20, 19, 21]. The main idea is to formulate an operator equation describing a chart or covering map for the desired manifold. This is usually done by considering a dynamical conjugacy characterizing the desired manifold. The present section reviews the parameterization method only as used in the remainder of the present work: namely for one dimensional local stable/unstable manifolds of planar analytic maps. The primary reference for the material in this section is [30], however the reader interested in a much more complete treatment of the parameterization method can refer to the recent book on the topic [22]. In particular the book contains an exhaustive overview of the literature.

Consider a smooth one parameter family of diffeomorphisms $f\colon \mathbb{R}^2 \times \mathbb{R} \to \mathbb{R}^2$. Let $U = (\lambda_1 - \epsilon, \lambda_1 + \epsilon)$ and suppose that $p\colon U \to \mathbb{R}^2$ is a smooth branch of hyperbolic fixed points. Let $\kappa_u, \kappa_s\colon U \to \mathbb{R}$ denote smooth branches of eigenvalues, and $\xi_u, \xi_s\colon U \to \mathbb{R}^2$ denote assocated smooth branches of eigenvectors.

We focus momentarily on the unstable manifold. The parameterization method seeks a function $P\colon (-1,1) \times U \to \mathbb{R}^2$ satisfying the conjugacy equation

$$f(P(\theta,\lambda)) = P(\kappa_u(\lambda)\theta), \tag{2}$$

for all $\theta \in (-1,1)$, and subject to the first order constraints

$$P(0,\lambda) = p(\lambda), \qquad \text{and} \qquad \frac{\partial}{\partial\theta} P(0,\lambda) = \xi_u(\lambda).$$

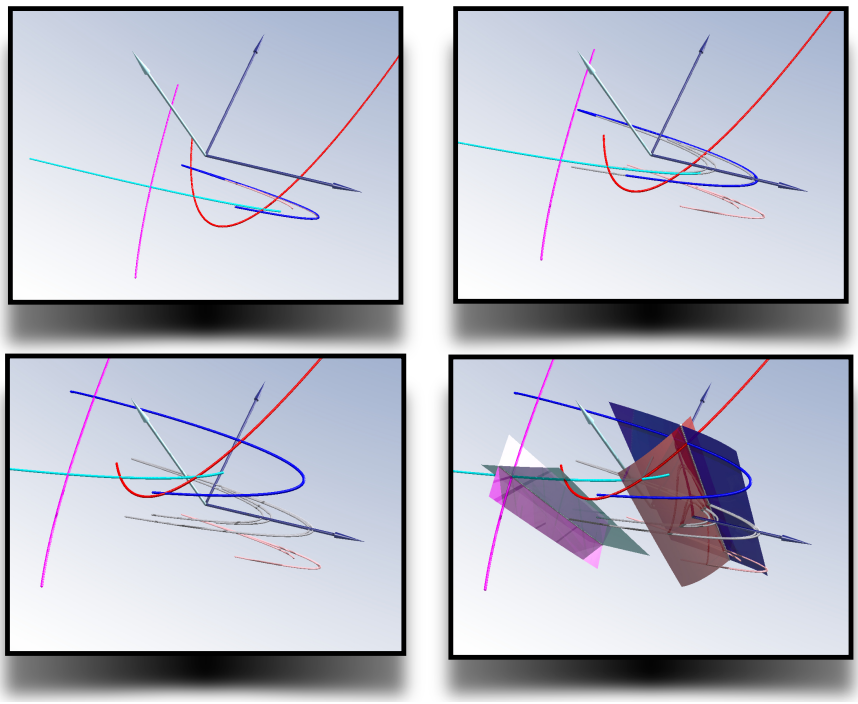

Figure 2: The figure illustrates the dynamics of the Hénon map at three different parameter values. In each of the four windows the $x - y$ axes are the phase space variables for the Hénon map. The parameter λ is on the z axis. The coordinate frame is based at the classical parameter values of the system, i.e. at $\lambda = 0$. In the top left frame we see the stable/unstable manifolds of the two fixed points of Hénon, when the parameter has $\lambda = -0.2$. Note for example that the red (stable) and blue (unstable) manifolds intersect transversally, giving rise to a homoclinic connecting orbit. The top right frame illustrates the dynamics at $\lambda = 0$ and again there appear to be homoclinic connections (the shadow of the attractor at $\lambda = -0.2$ remains). The bottom left frame illustrates the dynamics at $\lambda = 0.2$ (with the shadows of the two previous attractors). The homoclinic connection seems to persist for all $\lambda \in [-0.2, 0.2]$. The bottom right frame illustrates the one parameter families of local stable/unstable manifolds for the entire parameter interval. These manifolds are critical in our continuation and bifurcation analysis for connecting orbits.

Such a function P parameterizes a local unstable manifold for f at p. Figure 3 illustrates the meaning of Equation 2 for a fixed parameter value. Figure 4 illustrates the meaning of the parameter dependance.

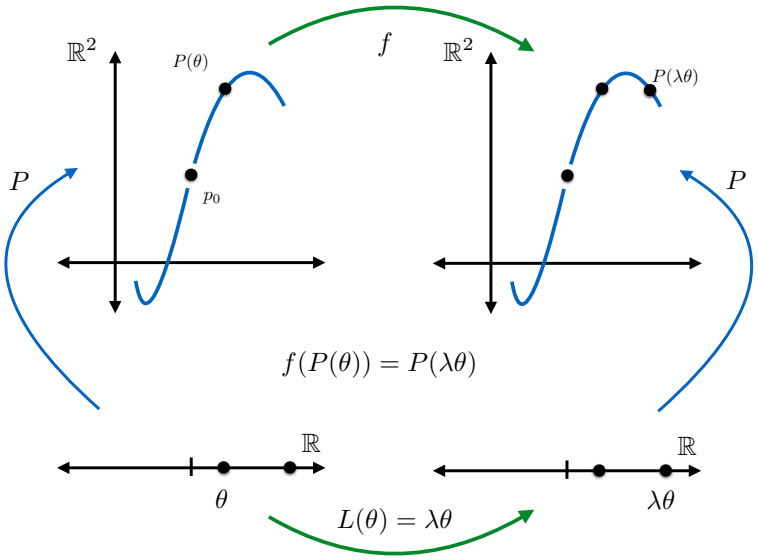

Figure 3: graphical illustration of the conjugacy relation exploited in the formulation of the parameterization method. A map P is sought which conjugates the linear dynamics in the parameter space to the nonlinear dynamics restricted to the local manifold.

2.1 Formal series expansions

To compute a numerical approximation of P solving Equation (2) we exploit power series methods. If f is analytic then p, $\kappa_{u,s}$, $\xi_{u,s}$, and P depend analytically on λ. So, let

$$p(\lambda) = \sum_{m=0}^{\infty} p_m \lambda^m, \qquad \kappa_u = \sum_{m=0}^{\infty} \kappa_m \lambda^m, \qquad \text{and} \qquad \xi_u(\lambda) = \sum_{m=0}^{\infty} \xi_m \lambda^m,$$

denote the power series expansions. We also write

$$\kappa_u^n(\lambda) = \sum_{m=0}^{\infty} \kappa_{mn} \lambda^m,$$

to denote the power series expansion of the eigenvalue raised to the n-th power. Methods for computing and validating these series expansions are discussed in [30].

We desire a solution P of equation (2) having power series expansion

$$P(\theta, \lambda) = \sum_{n=0}^{\infty} \sum_{m=0}^{\infty} p_{mn} \lambda^m \theta^n. \tag{3}$$

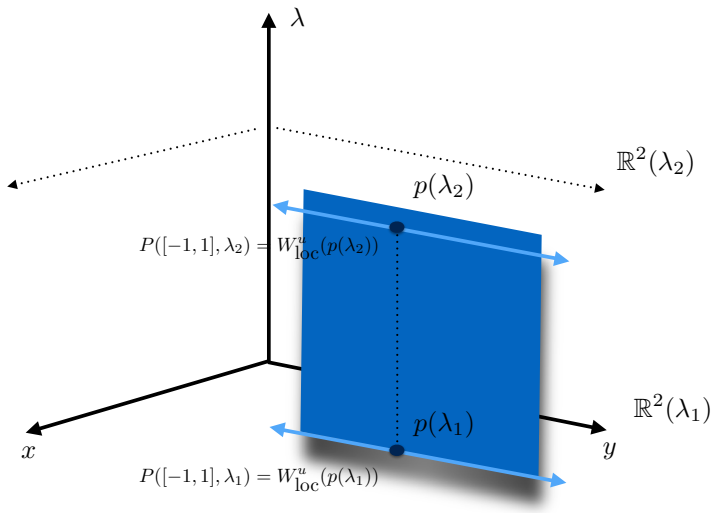

Figure 4: Branch of parameterized manifolds associated with a branch of hyperbolic fixed points.

Imposing the first order constraints gives

$$p_{0n} = p_n, \qquad \text{and} \qquad p_{1n} = \xi_n,$$

for all $n \in \mathbb{N}$. Using Equation (3) we expand Equation (2) as a power series, match like powers and solve for the n-th order coefficient. This leads to *homological equations* describing the coefficients p_{mn} when $n \geq 2$.

For example when f is the Hénon map defined in Equation (5) we have that

$$f(P(\theta,\lambda)) =$$

$$\begin{pmatrix} 1 + \sum_{m=0}^{\infty}\sum_{n=0}^{\infty} p^2_{mn}\lambda^m\theta^m - \lambda\sum_{m=0}^{\infty}\sum_{n=0}^{\infty}\sum_{j=0}^{m}\sum_{k=0}^{n} p^1_{m-j,n-k}p^1_{j,k}\lambda^m\theta^n \\ b\sum_{m=0}^{\infty}\sum_{n=0}^{\infty} p^1_{mn}\lambda^m\theta^n + \sum_{m=1}^{\infty}\sum_{n=0}^{\infty} p^1_{m-1,n}\lambda^m\theta^n \end{pmatrix},$$

and that

$$P(\kappa(\lambda)\theta,\lambda) = \sum_{n=0}^{\infty}\sum_{m=0}^{\infty}\sum_{k=0}^{m} \kappa_{m-k,n}\begin{pmatrix} p^1_{k,n} \\ p^2_{k,n}\end{pmatrix}\lambda^m\theta^m.$$

Setting these equal to one another and matching like powers of λ and θ gives

$$p^2_{mn} - \sum_{j=0}^{m}\sum_{k=0}^{n} \lambda p^1_{m-j,n-k}p^1_{j,k} = \kappa_{m-k,n}p_{k,n},$$

and

$$bp^1_{mn} + p^1_{m-1,n} = \kappa_{m-k,n}p_{k,n}.$$

Isolating the dependance on the $(m+n)$-th order term gives the *homological equation* for the coefficients

$$\begin{pmatrix} -2\lambda p^1_{00} - \lambda_0^n & 1 \\ b & -\lambda_0^n \end{pmatrix} \begin{bmatrix} p^1_{mn} \\ p^2_{mn} \end{bmatrix} = \begin{bmatrix} s^1_{mn} \\ s^2_{mn} \end{bmatrix}, \tag{4}$$

where

$$s^1_{mn} = \sum_{j=0}^{mn} \kappa_{m-j,n} p^1_{jn} + \sum_{k=0}^{n} \sum_{j=0}^{m} \lambda \hat{\delta}^{mn}_{jk} p^1_{m-j,n-k} p^1_{jk},$$

and

$$s^2_{mn} = -p^1_{m-1,n} + \sum_{j=0}^{m-1} \kappa_{m-j,n} p^2_{jn},$$

where

$$\hat{\delta}^{mn}_{jk} = \begin{cases} 0 & \text{if } j = m \text{ and } k = n \\ 0 & \text{if } j = 0 \text{ and } k = 0 \\ 1 & \text{otherwise} \end{cases}.$$

These expressions allow us to compute the Series solution $P(\theta, \lambda)$ to any desired finite order $m + n = N$. The manifold surfaces illustrated in Figures 5 and 2 are computed using these formulae.

Suppose now that

$$P^{MN}(\theta, \lambda) = \sum_{m=0}^{M} \sum_{n=0}^{N} \begin{pmatrix} p^1_{mn} \\ p^2_{mn} \end{pmatrix} \lambda^m \theta^n,$$

where the coefficients are the numerically computed solutions of the homological equation (4). The main result of [30] is that there exist $\tau, r > 0$ and an analytic function $H\colon (-r, r) \times (-\tau, \tau) \to \mathbb{R}^2$, so that

$$P(\theta, \lambda) = P^{MN}(\theta, \lambda) + H(\theta, \lambda),$$

is an exact solution of the invariance equation (2). The results of [30] also provide explicit bounds of the form

$$\sup_{(\theta,\lambda) \in (-r,r) \times (-\tau,\tau)} \|H(\theta, \lambda)\| \leq \epsilon,$$

where $\epsilon > 0$ depends on $N, M \in \mathbb{N}$, and on estimates which involve only the map f, the fixed point, and its eigenvalues/eigenvectors. These bounds are quite technical and we refer the interested reader to [30]. In the remainder of the present work we use the results of [30] freely and without further comment.

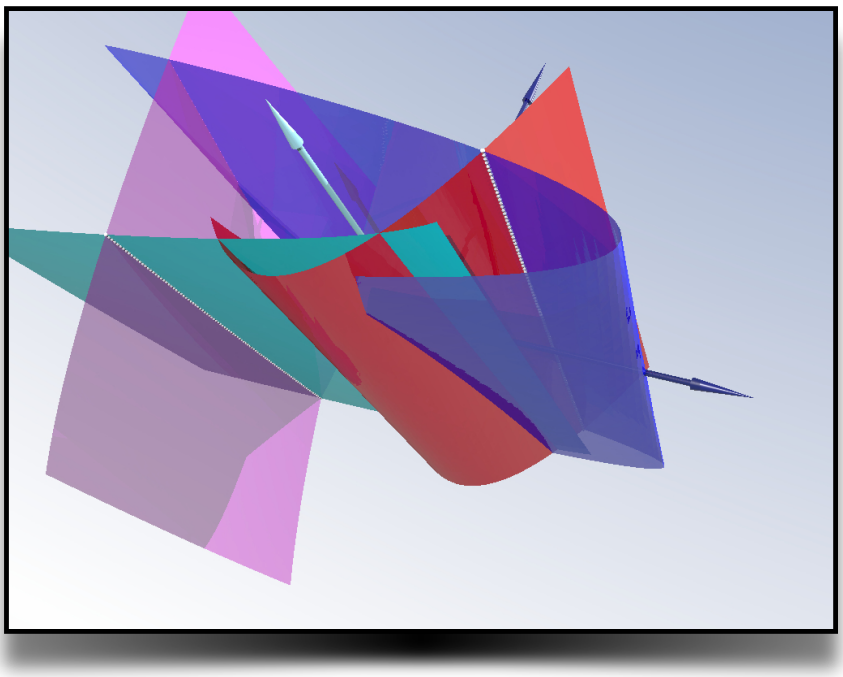

Figure 5: The figure illustrates larger local stable/unstable manifolds for the same parameters considered in Figure 2.

3 Connecting orbits: the method of projected boundaries

For a smooth diffeomorphism f on $\mathbb{R}^n$ with a hyperbolic fixed point $p \in \mathbb{R}^n$, a homoclinic orbit $(x_n)_{n\in\mathbb{Z}}$ based at p satisfies

$$x_{n+1} = f(x_n), \quad \lim_{n\to\pm\infty} x_n = p.$$

The authors of [5, 7, 6] use Newton's method to solve the system

$$\begin{aligned} &x_{n+1} = f(x_n),\ n = n_-, \ldots, n_+ - 1 \\ &b_-(x_{n_-}) = b_+(x_{n_+}) = 0. \end{aligned}$$

where the zero sets of b_- and b_+ are linear approximations to the local unstable and stable manifolds at the fixed point. We consider a slightly modified system

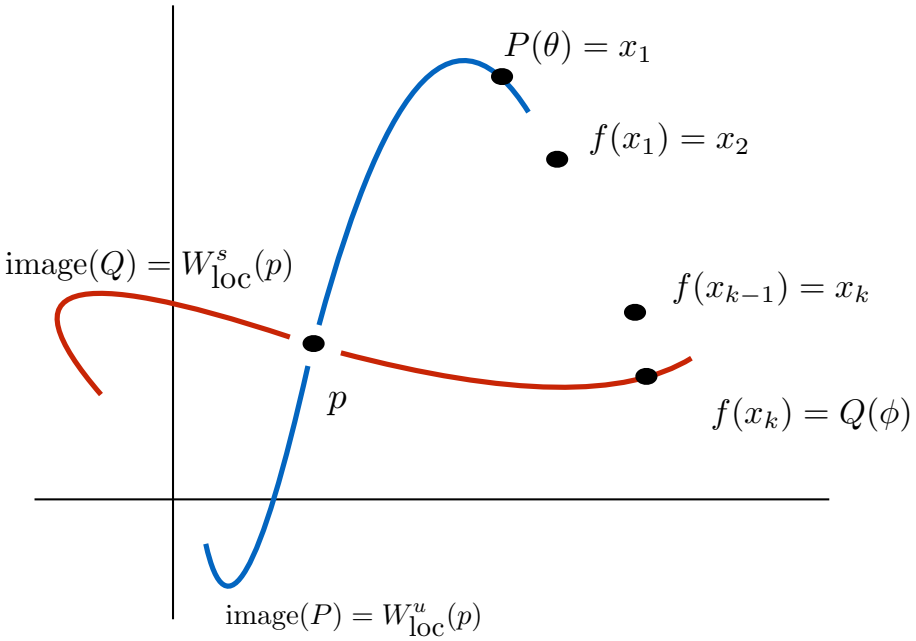

Figure 6: Graphical illustration of the multiple shooting scheme defining the connecting orbit operator.

and define the following *connecting orbit operator* $F : \mathbb{R}^{n(k+1)} \to \mathbb{R}^{n(k+1)}$

$$F(x, \theta, \phi) = \begin{bmatrix} f^{-1}(x_1) - Q(\theta) \\ \vdots \\ f(x_j) - x_{j+1} \\ \vdots \\ f(x_k) - P(\phi) \end{bmatrix}, \quad j = 1, \ldots, k-1.$$

Here P, Q are local parametrizations of the stable and unstable manifold, where $\theta \in W_u \subset \mathbb{R}^{n_u}$ and $\phi \in W_s \subset \mathbb{R}^{n_s}$ and $n_u + n_s = n$. It is then apparent that if $F(\tilde{x}, \tilde{\theta}, \tilde{\phi}) = 0$ then $\{\tilde{x}_i\}$ lies on a connecting orbit which is either homoclinic or heteroclinic depending on whether the local parametrization P is centered at p or another fixed point. The validation of the local parametrizations P and Q can be found in [32] where as the theory is developed in [15, 16, 17]. Let P be a parameterization for the stable manifold of $f : \mathbb{R}^n \to \mathbb{R}^n$ at p represented by

$P(\theta) = \sum_{|\alpha|>0} a_\alpha \theta^\alpha$. In what's to come revisit the *Hénon map* with parameters $a = 1.4$, $b = 0.3$:

$$H(a,b) \begin{cases} x_{n+1} = 1 - ax_n^2 + y_n \\ y_{n+1} = bx_n. \end{cases} \tag{5}$$

Recall that the computation of the coefficients a_α is done by exploiting the *conjugacy equation*

$$f(P(\theta)) = P(\Lambda_s \theta) \tag{6}$$

which leads to solving the following system (*homological equation*):

$$[Df(p) - (\lambda_1^{\alpha_1} \cdots \lambda_k^{\alpha_k})\mathrm{Id}]\, a_\alpha = s_\alpha,\ |\alpha| \geq 2, \tag{7}$$

the terms $\lambda_1, \ldots, \lambda_k$ are the eigenvalues of the diagonal matrix Λ_s. Here the function s_α is in terms of the lower order coefficients a_β for $|\beta| < |\alpha|$. The system (7) is a linear system of equations involving only the local data p_0, $Df(p_0)$ and the stable eigenvalues $\lambda_1, \ldots, \lambda_k$. Note that in (7) a_α is well defined as long as

$$\lambda_1^{\alpha_1} \cdots \lambda_k^{\alpha_k} \neq \lambda_i,$$

that is there is no resonance in α. In the case of the *Hénon map* the homological equation is

$$s_n = \begin{pmatrix} a \sum_{k=1}^{n-1} a_{n-k}^1 a_k^1 \\ 0 \end{pmatrix}.$$

Having computed the coefficients a_α we can define the truncation error h_N for the power series P determined by an N^{th} order approximation P_N given by $h_N = P - P_N$. With this in mind we can recast the *connecting orbit operator* as

$$F(x,\theta,\phi) = \underbrace{\begin{bmatrix} f^{-1}(x_1) - Q_{N_u}(\theta) \\ \vdots \\ f^{-1}(x_j) - x_{j+1} \\ f(x_j) - x_{j+1} \\ \vdots \\ f(x_k) - P_{N_s}(\phi) \end{bmatrix}}_{F_N} + \underbrace{\begin{bmatrix} -h_u(\theta) \\ \vdots \\ 0 \\ 0 \\ \vdots \\ -h_s(\phi) \end{bmatrix}}_{H}, \tag{8}$$

where $x \in \mathbb{R}^{kn}$. The idea here is to find an approximate zero $\tilde{x} = (\tilde{x}_0, \tilde{\theta}, \tilde{\phi}) \in \mathbb{R}^{n(k+1)}$ of (8) using Newton's method, that is

$$\|F(\tilde{x})\| \approx 0.$$

Then using the methods in [27], in particular the radii polynomial approach we can establish existence of a true zero $x^* = (x_0^*, \theta^*, \phi^*)$ near $\tilde{x}$. Now we

are ready to rigorously compute a transverse homoclinic orbit for (5). For the paramater values $a = 1.4$, $b = 0.3$ the *Henón* map $H(1.4, 0.3)$ takes the form $f(x, y) = \langle f_1(x, y), f_2(x, y)\rangle$, where $f_1(x, y) = 1 - 1.4x^2 + y$, $f_2(x, y) = 0.3x$. The approximating connecting orbit operator F_N is computed to be

$$F_N\left(x_1, \ldots, x_n, \theta, \phi\right) = \begin{bmatrix} Q^1_{N_u}(\theta) - x_1 \\ Q^2_{N_u}(\theta) - x_2 \\ 1 - 1.4x_1^2 + x_2 - x_3 \\ 0.3x_1 - x_4 \\ \vdots \\ 1 - 1.4x_{n-3}^2 + x_{n-2} - x_{n-1} \\ 0.3x_{n-3} - x_n \\ 1 - 1.4x_{n-1}^2 + x_n - P^1_{N_s}(\phi) \\ 0.3x_{n-1} - P^2_{N_s}(\phi) \end{bmatrix}$$

Given an initial guess $\bar{x}$ with $\|F_N(\bar{x})\| \approx 0$, we compute the $2(n+2) \times 2(n+2)$ Jacobian matrix

$$DF_N(\bar{x}) = \begin{pmatrix} -1 & 0 & 0 & \cdots & 0 & \frac{\partial Q^1_{N_u}(\bar{\theta})}{\partial \theta} & 0 \\ 0 & -1 & 0 & \cdots & 0 & \frac{\partial Q^2_{N_u}(\bar{\theta})}{\partial \theta} & 0 \\ -2.8\bar{x}_1 & 1 & -1 & 0 & \cdots & \cdots & 0 \\ 0.3 & 0 & 0 & -1 & 0 & \cdots & 0 \\ \vdots & \vdots & \vdots & \vdots & \ddots & \vdots & \vdots \\ 0 & 0 & \cdots & -2.8\bar{x}_{n-1} & 1 & 0 & \frac{\partial P^1_{N_s}(\bar{\phi})}{\partial \phi} \\ 0 & 0 & \cdots & 0.3 & 0 & 0 & \frac{\partial P^2_{N_s}(\bar{\phi})}{\partial \phi} \end{pmatrix}. \quad (9)$$

Set $A = [DF_N(\bar{x})]^{-1}$, and let $T(x) := x - AF_N(x)$. To apply the radii polynomial approach we compute the bounds Y, $Z(r)$ satisfying Theorem 2 in [27]. To determine Y note that

$$T(\bar{x}) - \bar{x} = -AF_N(\bar{x}) = -\left[DF_N(\bar{x})\right]^{-1} F_N(\bar{x}).$$

With this in mind we can compute $Y = (Y_1, \ldots, Y_n)$ such that $|[T(\bar{x}) - \bar{x}]_k| \leq Y_k$. Furthermore we determine $Z(r)$ such that

$$\sup_{b,c \in \overline{B_r(0)}} |DT_k(\bar{x} + b)c| \leq Z_k(r), \quad k = 1, \ldots, n.$$

In order to simplify the computation of Z_k we rescale the variables b and c. For $r > 0$, let $\tilde{b} := \frac{b}{r}$, $\tilde{c} := \frac{c}{r}$, with this the bounds become

$$\sup_{\tilde{b},\tilde{c} \in \overline{B_1(0)}} \left| DT_k(\bar{x} + \tilde{b})\tilde{c} \right| \leq Z_k(r), \quad k = 1, \ldots, n.$$

To simplify some of the technical estimates we consider the splitting

$$\begin{aligned} DT(\bar{x}+\tilde{b}r)\tilde{c}r &= \left(I - ADF_N(\bar{x}+\tilde{b}r)\tilde{c}r\right) \\ &= \left(I - ADF_N(\bar{x})\right)\tilde{c}r - A\left(DF_N(\bar{x}+\tilde{b}r) - DF_N(\bar{x})\right)\tilde{c}r \\ &= -A\left(DF_N(\bar{x}+\tilde{b}r) - DF_N(\bar{x})\right)\tilde{c}r. \end{aligned}$$

where $A = DF_N(\bar{x})^{-1}$. To bound the second term in the splitting we note that

$$\left(DF_N(\bar{x}+\tilde{b}r) - DF_N(\bar{x})\right)\tilde{c}r = \left(D^2F_N((1-t)\bar{x}+t(\bar{x}+\tilde{b}r))\cdot\tilde{b}\right)\tilde{c}r^2,$$

for some $t \in (0,1)$. Since the map is quadratic in $(x_1,\ldots,x_n)$ and we have uniform bounds for the manifold parametrizations the above expression can be bounded as follows

$$\left|DF_N(\bar{x}+\tilde{b}r) - DF_N(\bar{x})\right| \mathbb{1}_n r \leq \left(\sup\left|D^2F_N(\cdot)\mathbb{1}_n\right|\right)\mathbb{1}_n r^2. \tag{10}$$

To obtain the appropriate bounds for the manifold parametrizations in (10) we appeal to the Cauchy estimates in [32]. Set

$$Z_i(r) = \left[\left(\sup\left|D^2F_N(\cdot)\mathbb{1}_n\right|\right)\mathbb{1}_n\right]_i, \quad i = 1,\ldots,n.$$

Therefore the radii polynomials are defined to be

$$p_i(r) = Z_i(r)r^2 - r + Y_i.$$

For instance using Newton's method we can compute the following initial approximation

$$\bar{\mathbf{x}} = \begin{bmatrix} 1.098047712593213 \\ 0.093536312288055 \\ -0.594455978495608 \\ 0.329414313777964 \\ 0.834685239261125 \\ -0.178336793548682 \\ -0.153716021645244 \\ 0.250405571778337 \\ 1.217325510343720 \\ -0.046114806493573 \\ -1.120748763880612 \\ 0.365197653103116 \\ -0.393311255332770 \\ -0.336224629164183 \\ 0.447204129835801 \\ -0.117993376599831 \\ -0.584124438458463 \\ 0.063853585141195 \end{bmatrix}$$

with a tolerance $\epsilon = 10^{-15}$, that is $\|F_N(\bar{x})\| < \epsilon$. The interval containing all admissible radii values for existence is

$$I = \left[7.226661139604260 \times 10^{-6}, 0.041281531052901\right].$$

4 Continuation of connecting orbits

In many applications it is important to allow for a parameter in the map being studied, therefore we consider the problem of finding connecting orbits for

$$f(x, \lambda),$$

where $f : \mathbb{R}^n \times \mathbb{R}^m \to \mathbb{R}^n$. Given a connecting orbit of f, which is a zero of the corresponding connecting orbit map F, that is $F(x_0, \lambda_0) = 0$, we can try to find a continuous parametrized function $\alpha : V \to \mathbb{R}^n$ where $V \subset \mathbb{R}^m$ is a neighborhood of λ_0 such that $\alpha(\lambda_0) = x_0$ with $f(\alpha(\lambda), \lambda) = 0$. This amounts to an application of the implicit function theorem. In this section we consider examples with $m = 1$ and consider the following IVP

$$\frac{d\alpha}{d\lambda} = G(\alpha, \lambda) := -\left[D_x F(\alpha, \lambda)\right]^{-1} \frac{\partial F}{\partial \lambda}(\alpha, \lambda), \quad \alpha(\lambda_0) = x_0, \quad F(x_0, \lambda_0) = 0. \tag{11}$$

If $D_x F(x, \lambda)$ is invertible and G is smooth then by standard existence/uniqueness results there exists a smooth solution $\alpha : J \to \mathbb{R}^n$ where $J \subset \mathbb{R}$ is a neighborhood of λ_0. From (11)

$$\begin{aligned} D_x F(x, \lambda) \frac{d\alpha}{d\lambda} + \frac{\partial F}{\partial \lambda}(x, \lambda) &= 0 \\ \frac{d}{d\lambda} F(\alpha, \lambda) &= 0 \\ F(\alpha, \lambda) &= f(\alpha(\lambda_0), \lambda_0). \end{aligned}$$

Since we assume $F(\alpha(\lambda_0), \lambda_0) = 0$ we have that $F(\alpha(\lambda), \lambda) = 0$. Now computing the exact form of α can be an arduous task, but using that α is a solution to the differential equation (11) we can compute an approximation to α using the standard Euler approximation and set

$$x_1 := x_0 + hG(x_0, \lambda_0) \tag{12}$$

$$\lambda_1 := \lambda_0 + h, \tag{13}$$

where $|h| > 0$ is a sufficiently small step size. With this choice of h, we can then expect that $\|F(x_1, \lambda_1)\| \approx 0$, which would then lead to the Newton operator

$$T(x) := x - \left[D_x F(x_1, \lambda_1)\right]^{-1} F(x, \lambda_1)$$

being a contraction mapping, that is $0 \leq \|F(T(x_1), \lambda_1)\|_\infty \leq \|F(x_1, \lambda_1)\|_\infty$ which shows that $T(x_1)$ is a better approximation of a zero of F at λ_1 than x_1.

What we have essentially done is execute a *predictor-corrector* method where Euler's method is used to predict a new root and Newton's method is used to improve upon the guess.

The goal of this section is to rigorously compute branches of connecting orbits for the map $f : \mathbb{R}^n \times \Lambda \to \mathbb{R}^n$ with $\Lambda \subset \mathbb{R}$. We also assume that $f \in C^1(\mathbb{R}^n \times \Lambda, \mathbb{R}^n)$. Given two approximate zeros of $F(x, \lambda)$ say $(\bar{x}_0, \lambda_0)$ and $(\bar{x}_1, \lambda_1)$, let

$$\lambda_s := (1-s)\lambda_0 + s\lambda_1$$
$$\bar{x}_s := (1-s)\bar{x}_0 + s\bar{x}_1.$$

We look to obtain existence of a smooth branch of zeros $\tilde{x}_s$ of $F(x, \lambda)$ centered about the segment $\{\bar{x}_s : s \in [0,1]\}$, to accomplish this we use the method of radii polynomials. The existence theorems used in this section can be found in [27], for completeness we state the main existence theorem below. Set

$$B_r := \bigcup_{s\in[0,1]} \overline{B_r(\bar{x}_s)} \times \{\lambda_s\},$$

and define

(i) $T : \mathbb{R}^n \times [0,1] \to \mathbb{R}^n$ to be a Newton like operator $T(x,s) := x - AF(x, \lambda_s)$, where $A \in M_n(\mathbb{R})$.

(ii) For $k = 1, \ldots, n$, define $p_k(r) := Y_k + Z_k(r) - r$ where Y_k and $Z_k(r)$ satisfy $|[T(x_s, s) - x_s]_k| \leq Y_k$ and $\sup_{b,c\in\overline{B_r(0)}} |D_x T_k(x_s + b, s)c| \leq Z_k(r)$.

Theorem 4.1. *If there exists $r_0 > 0$, such that $p_k(r_0) < 0$, for all $k = 1, \ldots, n$, and $D_x f(x, \lambda)$ is invertible on B_{r_0}, then there exists a C^{m-1} function $\alpha : [\lambda_0, \lambda_1] \to B_{r_0}$ such that*

$$f(\alpha(\lambda), \lambda) = 0$$

and if $(x, \lambda) \in B_{r_0}$ and $f(x, \lambda) = 0$ then $x = \alpha(\lambda)$.

We demonstrate the above method for the *Henón* map (5), and rigorously compute the continuation of homoclinic orbits of length $L = 18$ from $\lambda_0 = 1.4$, to $\lambda_1 = 1.39$. Using the *predictor-corrector* technique we compute two approximate zeros of the corresponding connecting orbit operator F_N. That is,

$F_N(\bar{\mathbf{x}}_0, 1.4) \approx 0$, $F_N(\bar{\mathbf{x}}_1, 1.39) \approx 0$:

$$\bar{\mathbf{x}}_0 = \begin{bmatrix} 0.697104803703169 \\ 0.178872094163719 \\ 0.498534943879270 \\ 0.209131441110951 \\ 0.861179514734761 \\ 0.149560483163781 \\ 0.111278263925464 \\ 0.258353854420428 \\ 1.241017861589257 \\ 0.033383479177639 \\ -1.122791986719361 \\ 0.372305358476777 \\ -0.392621225140918 \\ -0.336837596015808 \\ 0.447350406980574 \\ -0.117786367542275 \\ -0.067765334076366 \\ 0.063801544981247 \end{bmatrix}, \quad \bar{\mathbf{x}}_1 = \begin{bmatrix} 0.700812984057372 \\ 0.178971787636650 \\ 0.496288801950127 \\ 0.210243895217212 \\ 0.867883316049093 \\ 0.148886640585038 \\ 0.101908824700883 \\ 0.260364994814728 \\ 1.245929276927566 \\ 0.030572647410265 \\ -1.127179623306027 \\ 0.373778783078270 \\ -0.392263342364612 \\ -0.338153886991808 \\ 0.447966076637543 \\ -0.117679002709384 \\ -0.069964960798780 \\ 0.064215201584631 \end{bmatrix}$$

Following the radii polynomial approach we first determine the bound Y_k by noting that

$$|[T(x_s, s) - x_s]_k| = |[AF(\bar{x}_s, \lambda_s)]_k|,$$

here we use the numerically computed inverse $A \approx D_x F_N(\bar{x}_0, \lambda_0)^{-1}$. To simplify this expression we define $g : [0,1] \to \mathbb{R}^{18}$ by $g(s) = F(\bar{x}_s, \lambda_s)$, expanding about zero yields

$$\begin{aligned} g(s) &= g(0) + g'(0)s + \frac{1}{2}g''(0)s^2 + \frac{1}{6}g'''(s^*)s^3 \\ &= F(\bar{x}_0, \lambda_0) + [D_x F(\bar{x}_0, \lambda_0)(\bar{x}_1 - \bar{x}_0) + D_\lambda F(\bar{x}_0, \lambda_0)(\lambda_1 - \lambda_0)]\, s \\ &+ \frac{1}{2}\left[D_x^2 F(\bar{x}_0, \lambda_0)(\bar{x}_1 - \bar{x}_0, \bar{x}_1 - \bar{x}_0) + 2D_{x,\lambda}F(\bar{x}_0, \lambda_0)(\bar{x}_1 - \bar{x}_0)(\lambda_1 - \lambda_0)\right. \\ &\left. + D_\lambda^2 F(\bar{x}_0, \lambda_0)(\lambda_1 - \lambda_0)^2\right] s^2 + \frac{1}{6}\left[D_x^3 F(\bar{x}_{s^*}, \lambda_{s^*})(\bar{x}_1 - \bar{x}_0)^3\right. \\ &+ 2D_{xx,\lambda}F(\bar{x}_{\delta^*}, \lambda_{s^*})(\bar{x}_1 - \bar{x}_0, \bar{x}_1 - \bar{x}_0)(\lambda_1 - \lambda_0) \\ &+ 2D_{x,\lambda\lambda}F(\bar{x}_{s^*}, \lambda_{s^*})(\bar{x}_1 - \bar{x}_0)(\lambda_1 - \lambda_0)^2 \\ &\left. + D_\lambda^3 F(\bar{x}_{s^*}, \lambda_{s^*})(\lambda_1 - \lambda_0)^3\right] s^3, \end{aligned}$$

where $s^* \in (0, s)$. The reason for the third order expansion is due to the fact that for $i = 3, \ldots, L-2$ the i^{th} coordinate function $F^{(i)}$ is at most cubic in s. To deal with the parametrizations P and Q we use the Cauchy estimate found

in [32], in particular Lemma 2.9. Returning to the Y_k bounds, set

$$
\begin{aligned}
y^{(0)} &:= F(\bar{x}_0, \lambda_0) \\
y^{(1)} &:= D_x F(\bar{x}_0, \lambda_0)(\bar{x}_1 - \bar{x}_0) + D_\lambda F(\bar{x}_0, \lambda_0)(\lambda_1 - \lambda_0) \\
y^{(2)} &:= \frac{1}{2}\left[D_x^2 F(\bar{x}_0, \lambda_0)(\bar{x}_1 - \bar{x}_0, \bar{x}_1 - \bar{x}_0) + 2D_{x,\lambda} F(\bar{x}_0, \lambda_0)(\bar{x}_1 - \bar{x}_0)(\lambda_1 - \lambda_0)\right. \\
&\left. + D_\lambda^2 F(\bar{x}_0, \lambda_0)(\lambda_1 - \lambda_0)^2\right] \\
y^{(3)} &:= \frac{1}{6}\left[D_x^3 F(\bar{x}_{s^*}, \lambda_{s^*})(\bar{x}_1 - \bar{x}_0)^3\right. \\
&+ 2D_{xx,\lambda} F(\bar{x}_{s^*}, \lambda_{\delta^*})(\bar{x}_1 - \bar{x}_0, \bar{x}_1 - \bar{x}_0)(\lambda_1 - \lambda_0) \\
&\left. + 2D_{x,\lambda\lambda} F(\bar{x}_{s^*}, \lambda_{\delta^*})(\bar{x}_1 - \bar{x}_0)(\lambda_1 - \lambda_0)^2 + D_\lambda^3 F(\bar{x}_{s^*}, \lambda_{s^*})(\lambda_1 - \lambda_0)^3\right].
\end{aligned}
$$

Therefore,

$$
|T(x_s, s) - x_s| = |AF(\bar{x}_s, \lambda_s)| \ll \left|Ay^{(0)}\right| + \left|Ay^{(1)}\right| + \left|Ay^{(2)}\right| + \left|Ay^{(3)}\right|.
$$

Hence we take Y to be $Y = (Y_1, Y_2, Y_3, Y_4)$ satisfying

$$
\left|Ay^{(0)}\right| + \left|Ay^{(1)}\right| + \left|Ay^{(2)}\right| + \left|Ay^{(3)}\right| \ll Y,
$$

the above bounds are computed using interval arithmetic. Next let us consider the Z_k bounds in Theorem 4.1.

$$
\begin{aligned}
D_x T(\bar{x}_s + b, s)c &= \left[I - AD_x F(\bar{x}_s + b, \lambda_s)\right] c \\
&= \left[I - AD_x F(\bar{x}_0 + (\bar{x}_1 - \bar{x}_0)s + b, \lambda_0 + (\lambda_1 - \lambda_0)s)\right] c \\
&= \left[I - AD_x F(\bar{x}_0, \lambda_0) + AD_x F(\bar{x}_0, \lambda_0)\right. \\
&\left. - AD_x F(\bar{x}_0 + (\bar{x}_1 - \bar{x}_0)s + b, \lambda_0 + (\lambda_1 - \lambda_0)s)\right] c. \qquad (14)
\end{aligned}
$$

Again we make use of the fact that for $i = 3, \ldots, L-2$, F^i is at most cubic in s, therefore we consider the Taylor expansion of $D_x F(x, \lambda)$ centered at $(\bar{x}_0, \lambda_0)$

$$
\begin{aligned}
&D_x F(\bar{x}_0 + (\bar{x}_1 - \bar{x}_0)s + b, \lambda_0 + (\lambda_1 - \lambda_0)s) \\
&= D_x F(\bar{x}_0, \lambda_0) + D_{xx}^2 F(\bar{x}_0, \lambda_0)((\bar{x}_1 - \bar{x}_0)s + b) + D_{x\lambda}^2 F(\bar{x}_0, \lambda_0)(\lambda_1 - \lambda_0)s \\
&+ \frac{1}{2} D_{xxx}^3 F(\bar{x}_{s^*}, \lambda_{s^*})((\bar{x}_1 - \bar{x}_0)s + b, (\bar{x}_1 - \bar{x}_0)s + b) \\
&+ D_{xx\lambda}^3 F(\bar{x}_{s^*}, \lambda_{s^*})(\bar{x}_1 - \bar{x}_0)s + b)(\lambda_1 - \lambda_0)s + \frac{1}{2} D_{x\lambda\lambda}^3 F(\bar{x}_{s^*}, \lambda_{s^*})(\lambda_1 - \lambda_0)^2 s^2.
\end{aligned}
$$

Plugging this into (14) we get

$$
\begin{aligned}
D_x T(\bar{x}_s + b, s)c &= \left[I - AD_x F(\bar{x}_0, \lambda_0)\right] c + A\left[D_{xx}^2 F(\bar{x}_0, \lambda_0)((\bar{x}_1 - \bar{x}_0)s + b)\right] c \\
&+ A\left[D_{x\lambda}^2 F(\bar{x}_0, \lambda_0)(\lambda_1 - \lambda_0)s\right] c \\
&+ \frac{1}{2} A\left[D_{xxx}^3 F(\bar{x}_{s^*}, \lambda_{s^*})((\bar{x}_1 - \bar{x}_0)s + b, (\bar{x}_1 - \bar{x}_0)s + b)\right] c \\
&+ A\left[D_{xx\lambda}^3 F(\bar{x}_{s^*}, \lambda_{s^*})((\bar{x}_1 - \bar{x}_0)s + b)(\lambda_1 - \lambda_0)s\right] c \\
&+ \frac{1}{2} A\left[D_{x\lambda\lambda}^3 F(\bar{x}_{s^*}, \lambda_{s^*})(\lambda_1 - \lambda_0)^2 s^2\right] c.
\end{aligned}
$$

Using the above expression we can identify the linear and quadratic coefficients of the radii polynomials, for $r > 0$, let $\tilde{b} := \frac{b}{r}$, $\tilde{c} := \frac{c}{r}$.

$$\begin{aligned} Z^{(1)} := & \left| I - AD_x F(\bar{x}_0, \lambda_0) \right| \mathbb{1}_{18} + |A| \left| D^2_{xx} F(\bar{x}_0, \lambda_0)(\bar{x}_1 - \bar{x}_0) \right| \mathbb{1}_{18} \\ & + |A| \left| D^2_{x\lambda} F(\bar{x}_0, \lambda_0)(\lambda_1 - \lambda_0) \right| \mathbb{1}_{18} \\ & + |A| \left| D^3_{xx\lambda} F(\bar{x}_{s^*}, \lambda_{s^*})(\bar{x}_1 - \bar{x}_0)(\lambda_1 - \lambda_0) \right| \mathbb{1}_{18} + \\ & \frac{1}{2} |A| \left| D^3_{x\lambda\lambda} F(\bar{x}_{s^*}, \lambda_{s^*})(\lambda_1 - \lambda_0)^2 \right| \mathbb{1}_{18} + \\ & \frac{1}{2} |A| \left| D^3_{xxx} F(\bar{x}_{s^*}, \lambda_{s^*})((\bar{x}_1 - \bar{x}_0)s + \tilde{b}, (\bar{x}_1 - \bar{x}_0)s + \tilde{b}) \right| \mathbb{1}_{18}, \end{aligned}$$

and

$$Z^{(2)} := |A| \left| D^2_{xx} F(\bar{x}_0, \lambda_0) \mathbb{1}_{18} \right| \mathbb{1}_{18} + |A| \left| D^3_{xx\lambda} F(\bar{x}_{s^*}, \lambda_{s^*})(\lambda_1 - \lambda_0) \mathbb{1}_{18} \right| \mathbb{1}_{18}.$$

Note that for the third order terms $D_{xxx}F$, $D_{xx\lambda}F$, and $D_{x\lambda\lambda}F$ the only non constant entries come from the local parametrization functions. We need to handle the corresponding truncation error functions $h^i_N = P^i - P^i_N$, and $g^i_N = Q^i - Q^i_N$ for $i = 1, 2$. We again appeal to Lemma 2.9 in [32]

$$\left| D^3_{xx\lambda} h^i_N(\bar{x}_{s^*}, \lambda_{s^*}) \right| \leq \frac{8\pi^3}{\nu^2 \tau \sigma^2_\nu \sigma_\tau} \left\| h^i_N \right\|_\nu \tag{15}$$

$$\left| D^3_{x\lambda\lambda} h^i_N(\bar{x}_{s^*}, \lambda_{s^*}) \right| \leq \frac{8\pi^3}{\nu \tau^2 \sigma_\nu \sigma^2_\tau} \left\| h^i_N \right\|_\nu \tag{16}$$

$$\left| D^3_{xxx} h^i_N(\bar{x}_{s^*}, \lambda_{s^*}) \right| \leq \frac{8\pi^3}{\nu^3 \sigma^3_\nu} \left\| h^i_N \right\|_\nu, \tag{17}$$

Here ν and τ are the radii of convergence for $P_N(\theta, \lambda)$, σ_ν satisfies $e^{-\sigma_\nu}\nu = \frac{\bar{x}_0(L-1)+\nu}{2}$ and τ satisfies $e^{-\sigma_\tau}\tau = \frac{\bar{x}_0(L-1)+\tau}{2}$. We can compute analogous bounds for the truncation error g^i_N. Therefore using the above bounds for $Z^{(1)}$ and $Z^{(2)}$ we have for all $s \in [0, 1]$,

$$\sup_{b,c \in \overline{B_r}(0)} |D_x T(\bar{x}_s + b, s)c| \ll Z(r) := Z^{(1)} r + Z^{(2)} r^2.$$

The radii polynomials are then

$$p_k(r) = Z^{(2)}_k r^2 + (Z^{(1)}_k - 1)r + Y_k,$$

for $k = 1, \ldots, L$. The interval containing all admissible radii values for existence is

$$I = [0.020747185206871, 0.077337999636518].$$

Choosing $r_0 = 0.03$, we get that for each $s \in [0, 1]$ there is a homoclinic orbit $x_s \in \overline{B_{r_0}(\bar{x}_s)}$, that is $F(x_s, \lambda_s) = 0$.

5 Saddle-Node Bifurcation

In this section we consider the problem of rigourously computing saddle-node bifurcation points for the connecting orbit map F. Consider a C^1 function $F : \mathbb{R}^n \times \mathbb{R} \to \mathbb{R}^n$ which gives rise to a parameter dependent map

$$F(x, \lambda) = F_\lambda(x), \quad \lambda \in \mathbb{R}.$$

A parameter value $\bar{\lambda} \in \mathbb{R}$ is a *bifurcation point* if given any $\epsilon > 0$ there exists $\lambda \in \mathbb{R}$ such that $\left\|\bar{\lambda} - \lambda\right\| < \epsilon$ and $F_\lambda(x)$ is not topologically equivalent to $F_{\bar{\lambda}}(x)$. One can search for bifurcation points by observing changes in the eigenvalue structure of the linearization of F. Connecting orbits are solutions to $F(x, \lambda) = 0$. If $F(\tilde{x}, \tilde{\lambda}) = 0$ and $D_x F(\tilde{x}, \tilde{\lambda})$ is invertible then by the implicit function theorem there is a smooth family of connecting orbits $\tilde{x}(\lambda)$ in a neighborhood of $\tilde{\lambda}$. Where as if $D_x F(\tilde{x}, \tilde{\lambda})$ is singular then there must be a zero eigenvalue, here we consider the simplest possible case where the multiplicity of the zero eigenvalue is one.

Definition 5.1. Consider $f : \mathbb{R}^n \times \mathbb{R} \to \mathbb{R}^n$. A *saddle-node* for f is a point $(\tilde{x}, \tilde{\lambda}) \in \mathbb{R}^n \times \mathbb{R}$ such that

(i) $f(\tilde{x}, \tilde{\lambda}) = 0$, and

(ii) zero is an eigenvalue of $D_x F(\tilde{x}, \tilde{\lambda})$ with algebraic multiplicity one and all other eigenvalues have non-zero real parts.

Definition 5.2. Given $F : \mathbb{R}^n \times \mathbb{R} \to \mathbb{R}^n$ a *saddle-node bifurcation* occurs at the saddle-node $(\tilde{x}, \tilde{\lambda}) \in \mathbb{R}^n \times \mathbb{R}$ if the following conditions are met.

SNB1 There exists a smooth curve $g : (-\delta, \delta) \to \mathbb{R}^n \times \mathbb{R}$ denoted by $s \mapsto (g_1(s), g_2(s))$ such that $g(0) = (\tilde{x}, \tilde{\lambda})$ and $F(g_1(s), g_2(s)) = 0$.

SNB2 The curve defined by g has a quadratic tangency with $\mathbb{R}^n \times \{\tilde{\lambda}\}$ at $(\tilde{x}, \tilde{\lambda})$, that is

$$g_2(0) = \tilde{\lambda}, \quad g_2'(0) = 0, \quad \text{and} \quad g_2''(0) \neq 0.$$

SNB2 If $s \neq 0$ then $D_x F(g_1(s), g_2(s))$ is hyperbolic and if $\sigma(s)$ is the eigenvalue of $D_x F(g_1(s), g_2(s))$ that satisfies $\sigma(0) = 0$, then $\sigma'(0) \neq 0$.

The following theorem which is proved in [9] as Theorem 8.12 provides sufficient generic conditions for a saddle-node bifurcation to occur in n-dimensions.

Theorem 5.3. (Saddle-node bifurcation theorem). *Assume $F : \mathbb{R}^n \times \mathbb{R} \to \mathbb{R}^n$ is C^1, $(\tilde{x}, \tilde{\lambda}) \in \mathbb{R}^n \times \mathbb{R}$ is a saddle-node, and the kernel of $D_x F(\tilde{x}, \tilde{\lambda})$ is spanned by the vector $\tilde{v} \in \mathbb{R}^n$. If*

$$D_\lambda F(\tilde{x}, \tilde{\lambda}) \neq 0 \quad \textit{and} \quad D_x^2 F(\tilde{x}, \tilde{\lambda})(\tilde{v}, \tilde{v}) \neq 0$$

and both are not in the range of $D_xF(\tilde{x},\tilde{\lambda})$, then there is a saddle-node bifurcation at $(\tilde{x},\tilde{\lambda})$. Moreover, among all C^∞ one parameter families that have a saddle-node, those that undergo a saddle-node bifurcation form an open and dense subset.

The next lemma provides us with a way of checking if $u_1,\, u_2 \neq 0$, then they are not in the range of $D_xF(\tilde{x},\tilde{\lambda})$. See Lemma 4 in [27] for the proof.

Lemma 5.4. *Let $D : \mathbb{R}^n \to \mathbb{R}^n$ be a linear transformation with* $\dim(\ker(D))$=1. Then $\ker(D)^T = \langle w \rangle$, for some $w \in \mathbb{R}^n \setminus \{0\}$. Also, u is in the range of D if and only if $u \cdot w = 0$.

The above Theorem 5.3 provides us with sufficient conditions to guarantee the occurrence of a saddle-node bifurcation, together with Lemma 5.4 provides a process for finding a saddle-node. The following algorithm illustrates this process.

Algorithm 5.5. *Let $f : \mathbb{R}^n \times \mathbb{R} \to \mathbb{R}^n$ be smooth. Assume there exists $(\bar{x},\bar{\lambda}) \in \mathbb{R}^n \times \mathbb{R}$ and $\mu \in \sigma(D_xf(\bar{x},\bar{\lambda}))$ such that $f(\bar{x},\bar{\lambda}) \approx 0$ and $\mu \approx 0$. Perform the following steps.*

(i) Rigorously compute eigenpairs $\{(\tilde{\mu}_i,\tilde{v}_i) \mid i = 1,\dots,n\}$ such that $\tilde{\mu}_i \in \overline{B_{r_i}(\bar{\mu}_i)}$ where

$$0 \in \overline{B_{r_1}(\bar{\mu}_1)} \quad \text{and} \quad \overline{B_{r_i}(\bar{\mu}_i)} \cap i\mathbb{R} = \emptyset, \quad i = 2,\dots,n.$$

(ii) Verify that $\tilde{\mu}_1 = 0$.

(iii) Define $u^1 := D_\lambda f(\tilde{x},\tilde{\lambda})$ and $u^2 := D_x^2 f(\tilde{x},\tilde{\lambda})(\tilde{v},\tilde{v})$ and verify that

$$w^T u^i \neq 0, \quad i = 1, 2, \tag{18}$$

where $w \in \mathbb{R}^n \setminus \{0\}$ such that $w^T D_xf(\tilde{x},\tilde{\lambda}) = 0$.

If steps (i)-(iii) are carried out successfully, then a saddle-node bifurcation occurs at the saddle-node $(\tilde{x},\tilde{\lambda}) \in \overline{B_{\tilde{r}}(\bar{x},\bar{\lambda})}$ where $\tilde{r}$ is obtained explicitly in the verification of step (ii).

If the above algorithm is executed correctly one can verify that the hypotheses of Theorem 5.3 will be satisfied. Next we discuss the rigorous numerical procedure used to carry out the above steps. For step (i) we use the techniques found in section 3.1 in [27]. We assume that this computation is successful. For step (ii) we need to verify that $\tilde{\mu}_1 = 0$, from the first step we know that there is at most one zero eigenvalue, hence it is enough to prove the existence of an eigenvector v that lies in the kernel of $D_xf(\tilde{x},\tilde{\lambda})$. Observe that if it exists, then $v \in \mathbb{R}^n$, so we can obtain isolation by requiring that $\|v\| = 1$. This leads to a modified version of the original $f(x,\lambda) = 0$ problem. That is we need to prove existence of $X = (x,\lambda,v) \in \mathbb{R}^{2n+1}$ satisfying

$$F(X) := \begin{pmatrix} f(x,\lambda) \\ \|v\|^2 - 1 \\ D_xf(x,\lambda)v \end{pmatrix} = 0. \tag{19}$$

To deal with the manifold parametrizations we consider the approximate map F_N defined by

$$F_N(X) := \begin{pmatrix} f_N(x,\lambda) \\ \|v\|^2 - 1 \\ D_x f_N(x,\lambda)v \end{pmatrix} \tag{20}$$

where f_N is the N^{th} order approximating connecting orbit map. The existence of such a zero can be addressed using the radii polynomial approach found in Section 3 in [27]. A solution to (19) yields the existence of $(\tilde{x},\tilde{\lambda}) \in \overline{B_{\tilde{r}}(\bar{x},\bar{\lambda})}$ for some $\tilde{r} > 0$. This completes the necessary action for step (ii).

Let $D := D_x f(\tilde{x},\tilde{\lambda})$, observe that step (iii) requires the existence of a vector $w \in \mathbb{R}^n \setminus \{0\}$ such that $w^T D = 0$. We next use the radii polynomial approach to compute rigorously a non-zero vector w such that $\ker(D^T) = \langle w \rangle$, therefore $\operatorname{rank}(D) = \operatorname{rank}(D^T) = n-1$. When it comes to solving $D^T w = 0$ we can delete a row from D^T and still retain the same solution space, to determine which row to delete we first assume that $\bar{v} \neq 0$ satisfies $D\bar{v} \approx 0$. Let k be the component of $\bar{v}$ with largest magnitude, that is

$$|\bar{v}_k| = \max_{i=1,\dots,n} \{|\bar{v}_i|\} \neq 0.$$

Let $C_1,\dots,C_n$ denote the columns of D and $R_1,\dots,R_n$ the corresponding rows of D^T that is $R_i = C_i^T$ for $i = 1,\dots,n$. Now from $D\bar{v} \approx 0$, we have

$$C_k \approx -\frac{1}{\bar{v}_k} \sum_{\substack{i=1 \\ i\neq k}} \bar{v}_i C_i \implies R_k = C_k^T \approx -\frac{1}{\bar{v}_k} \sum_{\substack{i=1 \\ i\neq k}} \bar{v}_i R_i.$$

We see that the k-th row R_k of D^T is a linear combination of the other rows, therefore we can delete it. Similarly we can get rid of the k-th column C_k of D. Set $M := \left(D_{\hat{k}}\right)^T$, where $D_{\hat{k}}$ is defined to be the $n \times (n-1)$ matrix defined by D without its k-th column C_k. A non-zero unit vector w such that $\ker D^T = \langle w \rangle$ is an isolated solution of

$$g(w) := \begin{pmatrix} \|w\|^2 - 1 \\ Mw \end{pmatrix} = 0, \tag{21}$$

which can be solved using the raddi polynomial approach outlined in [27]. To complete algorithm 5.5 we need to check that condition 18 holds, this can be done using interval arithmetic.

Example 5.6. To demonstrate the above procedure for rigorously computing saddle-node bifurcations we consider the *Henón* map. Using Newton's method we find an approximate zero to (20), that is $\bar{X} = (\bar{x},\bar{\lambda},\bar{v}) \in \mathbb{R}^{2(18)+1}$ and $F_N(\bar{X},\lambda,v) \approx 0$ where

$$\lambda = 1.385545413332598$$

$$x = \begin{pmatrix} 1.110073970005463 \\ 0.090690040004348 \\ -0.616667996483824 \\ 0.333022191001639 \\ 0.806127787762997 \\ -0.185000398945147 \\ -0.085386015573669 \\ 0.241838336328899 \\ 1.231736641101901 \\ -0.025615804672101 \\ -1.127730879179147 \\ 0.369520992330570 \\ -0.392583707924363 \\ -0.338319263753744 \\ 0.448137750767427 \\ -0.117775112377309 \\ -0.601606703835879 \\ 0.064478916318970 \end{pmatrix}, \quad v = \begin{pmatrix} 0.072802041543708 \\ -0.022651107912389 \\ -0.246598617827939 \\ 0.021840612463112 \\ -0.399557716364655 \\ -0.073979585348382 \\ 0.818573745001379 \\ -0.119867314909396 \\ 0.073817387140959 \\ 0.245572123500414 \\ -0.006385376328312 \\ 0.022145216142288 \\ 0.002190629726767 \\ -0.001915612898494 \\ 0.000467540566561 \\ 0.000657188918030 \\ -0.130588658178558 \\ -0.000166627203463 \end{pmatrix}.$$

Next we compute $D_X F_N(\bar{X})$,

$$D_X F_N(\bar{X}) = \begin{pmatrix} D_x f_N(\bar{x}, \bar{\lambda}) & D_\lambda f_N(\bar{x}, \bar{\lambda}) & 0 \\ 0 & 0 & 2\bar{v}^T \\ D_x \left(D_x f_N(\bar{x}, \bar{\lambda}) \right) & D_x D_\lambda f_N(\bar{x}, \bar{\lambda})\bar{v} & D_x f_N(\bar{x}, \bar{\lambda}) \end{pmatrix}$$

from this we use interval arithmetic to compute $A = D_X F_N(\bar{X})^{-1}$, this can be done in practice using INTLAB in MATLAB which means A will have interval entries. Define $T : \mathbb{R}^{37} \to \mathbb{R}^{37}$ by

$$T(X) := X - AF_N(X),$$

Thus the Y bound can be determined by $\left|AF(\bar{X})\right| \ll Y$. Next we compute the Z bound, for this we exploit the choice of A.

$$DT(\bar{X} + b)c = -A \left(DF_N(\bar{X} + b) - DF_N(\bar{X}) \right) c.$$

Defining $h : [0, 1] \to \mathbb{R}^{37}$ by $h(s) = D_X F \left(\bar{X} + sb \right) c$, then $h(1) - h(0) = \left(DF_N(\bar{X} + b) - DF_N(\bar{X}) \right) c$, hence for $k = 1, \ldots, 37$ there exists $s_k \in [0, 1]$ such that

$$\left(D_X F_N^k(\bar{X} + b) - DF_N^k(\bar{X}) \right) c = h(1) - h(0) = h_k'(s_k) = D_X^2 F_N^k(\bar{X} + s_k b)(b, c).$$

Where b, $c \in \overline{B_r(0)}$ we can write $b = \tilde{b}r$, $c = \tilde{c}r$ for $\tilde{b}$, $\tilde{c} \in \overline{B_1(0)}$. With this in mind we get

$$\left(D_X F_N^k(\bar{X} + b) - D_X F_N^k(\bar{X}) \right) c = D_X^2 F_N^k(\bar{X} + s_k b)(\tilde{b}, \tilde{c})r^2.$$

To assist in the computation of the Z-bound we set $r^* = 10^{-1}$ an a-priori upper bound for the right endpoint of the existence interval of the radii polynomials,

this assumption will be justified if we show that $r \leq r^*$. Denote by $\mathbf{b}^* = [-r^*, r^*]^{37}$ an interval vector in $\mathbb{R}^{37}$ with entries $[-r^*, r^*]$. Set $\mathbf{X}^* = \bar{x} + \mathbf{b}^*$ which has k^{th} entry equal to $\left[\bar{X}_k - r^*, \bar{X}_k + r^*\right]$, additionally we set $\boldsymbol{\delta} = [-1, 1]^{37}$. Then for b, $c \in B_r(0)$ we get that

$$\left|A(D_X F_N(\bar{X} + b) - D_X F_N(\bar{X}))c\right| \in \left|AD_X^2 F_N(\mathbf{X}^*)(\boldsymbol{\delta}, \boldsymbol{\delta})\right|.$$

Using interval arithmetic, we compute $Z \in \mathbb{R}^{37}$ such that

$$\left|AD_X^2 F(\boldsymbol{X}^*)(\boldsymbol{\delta}, \boldsymbol{\delta})\right| \ll Z^{(2)}.$$

With the above bounds we can compute the raddi polynomials as $p_k(r) = Z_k^{(2)} r^2 - r + Y_k$. Using interval arithmetic we compute the following existence interval

$$I = \left[7.626642783879959 \times 10^{-5}, 0.025005959509074\right].$$

We see that $0.025005959509074 < r^* = 10^{-1}$, hence the existence interval is valid. Applying Corollary 3 in [27] if we set $r = 7.7 \times 10^{-5}$ there exists a unique isolated $\tilde{X} = (\tilde{x}, \tilde{\lambda}, \tilde{v}) \in \overline{B_r(\bar{X})}$ such that $F(\tilde{X}) = 0$, with this we have $f(\tilde{x}, \tilde{\lambda}) = 0$ and dim(ker $D_x f(\tilde{x}, \tilde{\lambda})$)=1.

Let r be the smallest radius of existence for I, define $\mathbf{B}= \overline{B_r\left((\bar{x}, \bar{\lambda})\right)} \subset \mathbb{R}^{19}$ that is to say

$$\mathbf{B} = \prod_{k=1}^{16} \left[\bar{x}_k - r, \bar{x}_k + r\right] \times \left[\bar{\lambda} - r, \bar{\lambda} + r\right].$$

Let $D := D_x f(\tilde{x}, \tilde{\lambda})$ and $\mathbf{D}:= D_x f(\mathbf{B})$ a 18×18 interval matrix computed with interval arithmetic. Note that $D \subset \mathbf{D}$, we next use the radii polynomial for validating eigenvalue eigenvector pairs as outlined in Section 3.1 in [27] to show that $\sigma(\mathbf{D}) \subset \bigcup_{j=1}^{n} B_{r_j}$ for some small balls $B_{r_j} \in \mathbb{C}$. Note that the matrix $\mathbf{D}$ is a matrix with interval entries hence the bounds Y, Z_0 and Z_1 all have to bound the possible errors from $\mathbf{D}$ as well, we use interval arithmetic to accomplish this. We proved that the eigenvalues of $D_x f(\tilde{x}, \tilde{\lambda})$ are enclosed in $\bigcup_{j=1}^{10} B_{r_j}$ (see the table below), for $i = 11, \ldots, 18$ the eigenvalues are all equal to -1 which can be seen from the following Lemma.

Lemma 5.7. The matrix DF_N in (9) has the eigenvalue $\lambda = -1$ with multiplicity $n + 1$.

r_1	$4.977875660140754 \times 10^{-14}$
r_2	$5.572394561899415 \times 10^{-14}$
r_3	$1.077452764023203 \times 10^{-11}$
r_4	$1.115700402288748 \times 10^{-11}$
r_5	$9.140678188363738 \times 10^{-12}$
r_6	$8.765542069374511 \times 10^{-12}$
r_7	$8.597273938794502 \times 10^{-12}$
r_8	$8.151515612870005 \times 10^{-12}$
r_9	$8.565553368022381 \times 10^{-12}$
r_{10}	$8.548084306408510 \times 10^{-12}$

Proof.

$$\left|DF_N-\lambda I_{2(n+2)}\right|=\begin{vmatrix} -1-\lambda & 0 & 0 & \cdots & 0 & \frac{\partial Q^1_{N_u}(\bar\theta)}{\partial\theta} & 0 \\ 0 & -1-\lambda & 0 & \cdots & 0 & \frac{\partial Q^2_{N_u}(\bar\theta)}{\partial\theta} & 0 \\ -2.8\bar x_1 & 1 & -1-\lambda & 0 & \cdots & \cdots & 0 \\ 0.3 & 0 & 0 & -1-\lambda & 0 & \cdots & 0 \\ \vdots & \vdots & \vdots & \vdots & \ddots & \vdots & \vdots \\ 0 & 0 & \cdots & -2.8\bar x_{n-1} & 1 & -\lambda & \frac{\partial P^1_{N_s}(\bar\phi)}{\partial\phi} \\ 0 & 0 & \cdots & 0.3 & 0 & 0 & \frac{\partial P^2_{N_s}(\bar\phi)}{\partial\phi}-\lambda \end{vmatrix}$$

$$=(-1-\lambda)\begin{vmatrix} -1-\lambda & 0 & \cdots & 0 & \frac{\partial Q^2_{N_u}(\bar\theta)}{\partial\theta} & 0 \\ 1 & -1-\lambda & 0 & \cdots & \cdots & 0 \\ 0 & 0 & -1-\lambda & 0 & \cdots & 0 \\ \vdots & \vdots & \vdots & \vdots & \ddots & \vdots \\ 0 & \cdots & -2.8\bar x_{n-1} & 1 & -\lambda & \frac{\partial P^1_{N_s}(\bar\phi)}{\partial\phi} \\ 0 & \cdots & 0.3 & 0 & 0 & \frac{\partial P^2_{N_s}(\bar\phi)}{\partial\phi}-\lambda \end{vmatrix}$$

$$+\frac{\partial Q^1_{N_u}(\bar\theta)}{\partial\theta}\begin{vmatrix} 0 & -1-\lambda & 0 & \cdots & 0 & 0 \\ -2.8\bar x_1 & 1 & -1-\lambda & 0 & \cdots & \cdots \\ 0.3 & 0 & 0 & -1-\lambda & 0 & \cdots \\ \vdots & \vdots & \vdots & \vdots & \ddots & \vdots \\ 0 & 0 & \cdots & -2.8\bar x_{n-1} & 1 & \frac{\partial P^1_{N_s}(\bar\phi)}{\partial\phi} \\ 0 & 0 & \cdots & 0.3 & 0 & \frac{\partial P^2_{N_s}(\bar\phi)}{\partial\phi}-\lambda \end{vmatrix}.$$

Now

$$\begin{vmatrix} -1-\lambda & 0 & \cdots & 0 & \frac{\partial Q^2_{N_u}(\bar{\theta})}{\partial \theta} & 0 \\ 1 & -1-\lambda & 0 & \cdots & \cdots & 0 \\ 0 & 0 & -1-\lambda & 0 & \cdots & 0 \\ \vdots & \vdots & \vdots & \vdots & \ddots & \vdots \\ 0 & \cdots & -2.8\bar{x}_{n-1} & 1 & -\lambda & \frac{\partial P^1_{N_s}(\bar{\phi})}{\partial \phi} \\ 0 & \cdots & 0.3 & 0 & 0 & \frac{\partial P^2_{N_s}(\bar{\phi})}{\partial \phi} - \lambda \end{vmatrix}$$

$$= (-1-\lambda) \begin{vmatrix} -1-\lambda & 0 & \cdots & \cdots & 0 \\ 0 & -1-\lambda & 0 & \cdots & 0 \\ \vdots & \vdots & \vdots & \ddots & \vdots \\ 0 & -2.8\bar{x}_{n-1} & 1 & -\lambda & \frac{\partial P^1_{N_s}(\bar{\phi})}{\partial \phi} \\ 0 & 0.3 & 0 & 0 & \frac{\partial P^2_{N_s}(\bar{\phi})}{\partial \phi} - \lambda \end{vmatrix} + \frac{\partial Q^2_{N_u}(\bar{\theta})}{\partial \theta} \begin{vmatrix} 1 & -1-\lambda & 0 & \cdots & 0 \\ 0 & 0 & -1-\lambda & 0 & 0 \\ \vdots & \vdots & \vdots & \vdots & \vdots \\ 0 & \cdots & -2.8\bar{x}_{n-1} & 1 & \frac{\partial P^1_{N_s}(\bar{\phi})}{\partial \phi} \\ 0 & \cdots & 0.3 & 0 & \frac{\partial P^2_{N_s}(\bar{\phi})}{\partial \phi} - \lambda \end{vmatrix}.$$

The above determinants simplify as follows

(i)

$$\begin{vmatrix} -1-\lambda & 0 & \cdots & \cdots & 0 \\ 0 & -1-\lambda & 0 & \cdots & 0 \\ \vdots & \vdots & \vdots & \ddots & \vdots \\ 0 & -2.8\bar{x}_{n-1} & 1 & -\lambda & \frac{\partial P^1_{N_s}(\bar{\phi})}{\partial \phi} \\ 0 & 0.3 & 0 & 0 & \frac{\partial P^2_{N_s}(\bar{\phi})}{\partial \phi} - \lambda \end{vmatrix} = (-1-\lambda)^{2n} \begin{vmatrix} -\lambda & -\frac{\partial P^1}{\partial t} \\ 0 & -\frac{\partial P^2}{\partial t} - \lambda \end{vmatrix}$$

(ii)

$$\begin{vmatrix} 1 & -1-\lambda & 0 & \cdots & 0 \\ 0 & 0 & -1-\lambda & 0 & 0 \\ \vdots & \vdots & \vdots & \vdots & \vdots \\ 0 & \cdots & -2.8\bar{x}_{n-1} & 1 & \frac{\partial P^1_{N_s}(\bar{\phi})}{\partial \phi} \\ 0 & \cdots & 0.3 & 0 & \frac{\partial P^2_{N_s}(\bar{\phi})}{\partial \phi} - \lambda \end{vmatrix} = \begin{vmatrix} 0 & -1-\lambda & 0 & 0 & \cdots & 0 \\ -2.8x_3 & 1 & -1-\lambda & 0 & \cdots & 0 \\ 0.3 & 0 & 0 & -1-\lambda & \cdots & 0 \\ \vdots & \cdots & \cdots & \cdots & \ddots & \vdots \\ 0 & \cdots & 0 & -2.8x_{n-1} & 1 & \frac{\partial P^1_{N_s}(\bar{\phi})}{\partial \phi} \\ 0 & \cdots & 0 & 0.3 & 0 & \frac{\partial P^2_{N_s}(\bar{\phi})}{\partial \phi} - \lambda \end{vmatrix}$$

If we swap column $2k$ with column $2k-1$ for $k = 1, \ldots, n+1$ we obtain the matrix whose j^{th} diagonal entry is $-1-\lambda$ for $j = 2k-1$, $k = 1, \ldots, n$. Moreover the entries a_{ij} on the j^{th} column are zero for $i = 1, \ldots, j-1$ additionally the entries a_{jk} on the j^{th} row are zero for $k = j+1, \ldots, 2n+1$. Therefore computing the determinant by cofactor expansion will yield the factor $(-1-\lambda)^n$.

Similarly for the $(2n+3) \times (2n+3)$ determinant

$$\begin{vmatrix} 0 & -1-\lambda & 0 & \cdots & 0 & 0 \\ -2.8\bar{x}_1 & 1 & -1-\lambda & 0 & \cdots & \cdots \\ 0.3 & 0 & 0 & -1-\lambda & 0 & \cdots \\ \vdots & \vdots & \vdots & \vdots & \ddots & \vdots \\ 0 & 0 & \cdots & -2.8\bar{x}_{n-1} & 1 & \frac{\partial P^1_{N_s}(\bar{\phi})}{\partial \phi} \\ 0 & 0 & \cdots & 0.3 & 0 & \frac{\partial P^2_{N_s}(\bar{\phi})}{\partial \phi} - \lambda \end{vmatrix},$$

There will be a factor of the form $(-1-\lambda)^{n+1}$. ∎

We now complete the last part of Algorithm 5.5, let

$$\bar{w} = 10^{-3} \times \begin{pmatrix} -0.000584787583518 \\ -0.003307007663887 \\ -0.003307007663887 \\ -0.023468947133846 \\ -0.023468947133846 \\ -0.102328937598109 \\ -0.102328937598109 \\ -0.935962046666128 \\ -0.935962046666128 \\ 0.287414363345534 \\ 0.287414363345534 \\ 0.084019205675169 \\ 0.084019205675169 \\ 0.106052822225200 \\ 0.106052822225200 \\ -0.078384865790371 \\ -0.078384865790371 \\ 0.044313217450742 \end{pmatrix},$$

where $\bar{w}$ was numerically computed so that $D_x f(\bar{x}, \bar{\lambda})^T \bar{w} \approx 0$. As discussed above by choosing $D = D_x f(\tilde{x}, \tilde{\lambda})$ a nonzero vector $\bar{w}$ such that $\ker D^T = \langle w \rangle$ is an isolated solution to (21). Using the radii polynomial approach (c.f. Section 3 in [27]) we rigorously compute $\tilde{w} \in \overline{B_{4.46\times 10^{-16}}(\bar{w})}$ such that $D_x f(\tilde{x}, \tilde{\lambda})\tilde{w} = 0$.

Lastly define

$$u_1 = D_\lambda f(\tilde{x}, \tilde{\lambda}) \quad \text{and} \quad u_2 = D_x^2 f(\tilde{x}, \tilde{\lambda})(\tilde{v}, \tilde{v}),$$

we showed using interval arithmetic that $u_1 \cdot \tilde{w} \neq 0$ and $u_2 \cdot \tilde{w} \neq 0$.

Next we validate the saddle node bifurcations for the Hénon map appearing in the diagram below.

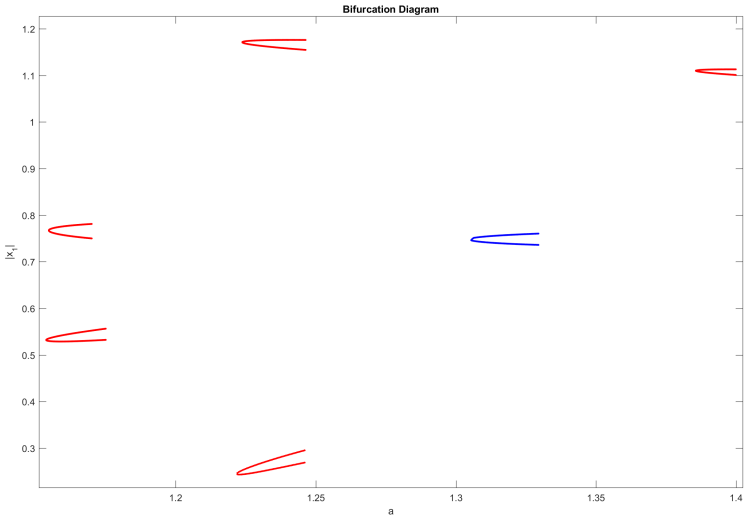

Figure 7: Saddle node bifurcations for the Hénon map.

The table below contains validated radii of existence for the saddle node bifurcation occurring at each parameter value a. Note that at $a = 1.385545413332598$

a	r_{eig}	r_{zero}	r_{ker}
1.15378575544751	3.42×10^{-13}	5.94×10^{-5}	3.66×10^{-16}
1.15498931237807	4.0×10^{-12}	4.25×10^{-5}	3.87×10^{-16}
1.22265205270066	6.0×10^{-13}	2.3×10^{-3}	3.3×10^{-16}
1.22376575784870	9.52×10^{-12}	4.75×10^{-5}	3.39×10^{-16}
1.30502761333254	9.8×10^{-12}	6.6×10^{-5}	3.86×10^{-16}

the saddle node bifurcation was validated in Example 5.6. Here r_{eig} denotes the uniform radius of existence for the eigenpair validation, r_{zero} denotes the uniform radius of existence for the zero of the map (19) which corresponds to the validation of $\tilde{\mu}_1 = 0$. Lastly r_{ker} denotes the radius of existence for the zero of the kernel map (21). Next we validate the branches of connecting orbits for each saddle node in figure 7.

a	r_{top}	r_{bottom}
$[1.385545413332598, 1.4]$	0.010190725482253	0.005284403661857
$[1.30502761333254, 1.33]$	0.013879617224993	0.009941633956819
$[1.22376575784870, 1.25]$	0.014682206461750	0.018859452169075
$[1.22265205270066, 1.246]$	0.013361275800433	0.017803702356127
$[1.15498931237807, 1.17]$	0.018581503663877	0.020369798040873
$[1.15378575544751, 1.175]$	0.026830304371292	0.026542006861268

Here r_{top}, r_{bottom} correspond to the radius of existence for the top branch and bottom branch of connecting orbits in figure 7 for the given range of parameter values a.

References

[1] Zin Arai. On hyperbolic plateaus of the Hénon map. *Experiment. Math.*, 16(2):181–188, 2007.

[2] Zin Arai. On loops in the hyperbolic locus of the complex Hénon map and their monodromies. *Phys. D*, 334:133–140, 2016.

[3] Zin Arai and Konstantin Mischaikow. Rigorous computations of homoclinic tangencies. *SIAM J. Appl. Dyn. Syst.*, 5(2):280–292 (electronic), 2006.

[4] Gianni Arioli and Hans Koch. Computer-assisted methods for the study of stationary solutions in dissipative systems, applied to the Kuramoto-Sivashinski equation. *Arch. Ration. Mech. Anal.*, 197(3):1033–1051, 2010.

[5] W.-J. Beyn. The numerical computation of connecting orbits in dynamical systems. *IMA J. Numer. Anal.*, 10(3):379–405, 1990.

[6] W.-J. Beyn and J.-M. Kleinkauf. Numerical approximation of homoclinic chaos. *Numer. Algorithms*, 14(1-3):25–53, 1997. Dynamical numerical analysis (Atlanta, GA, 1995).

[7] W.-J. Beyn and J.-M. Kleinkauf. The numerical computation of homoclinic orbits for maps. *SIAM J. Numer. Anal.*, 34(3):1207–1236, 1997.

[8] Maciej J. Capiński and J. D. Mireles James. Validated computation of heteroclinic sets. *SIAM J. Appl. Dyn. Syst.*, 16(1):375–409, 2017.

[9] Carmen Chicone. *Ordinary differential equations with applications*, volume 34. Springer,New York, second edition, 2006. Texts in Applied Mathematics.

[10] Sarah Day, Jean-Philippe Lessard, and Konstantin Mischaikow. Validated continuation for equilibria of PDEs. *SIAM J. Numer. Anal.*, 45(4):1398–1424, 2007.

[11] E. J. Doedel, B. W. Kooi, G. A. K. van Voorn, and Yu. A. Kuznetsov. Continuation of connecting orbits in 3D-ODEs. I. Point-to-cycle connections. *Internat. J. Bifur. Chaos Appl. Sci. Engrg.*, 18(7):1889–1903, 2008.

[12] E. J. Doedel, B. W. Kooi, G. A. K. Van Voorn, and Yu. A. Kuznetsov. Continuation of connecting orbits in 3D-ODEs. II. Cycle-to-cycle connections. *Internat. J. Bifur. Chaos Appl. Sci. Engrg.*, 19(1):159–169, 2009.

[13] Eusebius J. Doedel and Mark J. Friedman. Numerical computation of heteroclinic orbits. *J. Comput. Appl. Math.*, 26(1-2):155–170, 1989. Continuation techniques and bifurcation problems.

[14] J.-P. Eckmann, H. Koch, and P. Wittwer. A computer-assisted proof of universality for area-preserving maps. *Mem. Amer. Math. Soc.*, 47(289):vi+122, 1984.

[15] X. Cabré, E. Fontich, and R. de la Llave. The parameterization method for invariant manifolds. I. manifolds associated to non-resonant subspaces. *Indiana Univ. Math. J.*, 52:283–328, 2003.

[16] X. Cabré, E. Fontich, and R. de la Llave. The parameterization method for invariant manifolds. II. regularity with respect to parameters. *Indiana Univ. Math. J.*, 52:329–360, 2003.

[17] X. Cabré, E. Fontich, and R. de la Llave. The parameterization method for invariant manifolds. III. overview and applications. *J. Differential Equations*, 218:445–515, 2005.

[18] Jorge Gonzalez and J. D. Mireles James. High-order parameterization of stable/unstable manifolds for long periodic orbits of maps. *(To appear in SIAM Journal on Applied Dynaical Systems)*, pages 1–46, 2017.

[19] À. Haro and R. de la Llave. A parameterization method for the computation of invariant tori and their whiskers in quasi-periodic maps: numerical algorithms. *Discrete Contin. Dyn. Syst. Ser. B*, 6(6):1261–1300, 2006.

[20] A. Haro and R. de la Llave. A parameterization method for the computation of invariant tori and their whiskers in quasi-periodic maps: rigorous results. *J. Differential Equations*, 228(2):530–579, 2006.

[21] A. Haro and R. de la Llave. A parameterization method for the computation of invariant tori and their whiskers in quasi-periodic maps: explorations and mechanisms for the breakdown of hyperbolicity. *SIAM J. Appl. Dyn. Syst.*, 6(1):142–207, 2007.

[22] Àlex Haro, Marta Canadell, Jordi-Lluí s Figueras, Alejandro Luque, and Josep-Maria Mondelo. *The parameterization method for invariant manifolds*, volume 195 of *Applied Mathematical Sciences*. Springer, [Cham], 2016. From rigorous results to effective computations.

[23] Hans Koch, Alain Schenkel, and Peter Wittwer. Computer-assisted proofs in analysis and programming in logic: a case study. *SIAM Rev.*, 38(4):565–604, 1996.

[24] Oscar E. Lanford, III. Computer-assisted proofs in analysis. *Phys. A*, 124(1-3):465–470, 1984. Mathematical physics, VII (Boulder, Colo., 1983).

[25] Oscar E. Lanford, III. Computer-assisted proofs in analysis. In *Proceedings of the International Congress of Mathematicians, Vol. 1, 2 (Berkeley, Calif., 1986)*, pages 1385–1394. Amer. Math. Soc., Providence, RI, 1987.

[26] Jean-Philippe Lessard. Delay differential equations and continuation. *(Preliminary lecture notes for the AMS short course on rigorous numerics in dynamics)*, page `http://archimede.mat.ulaval.ca/jplessard/AMSnotes/`, 2016.

[27] Jean-Philippe Lessard. Rigorous verification of saddle-node bifurcations in ODEs. *Indag. Math. (N.S.)*, 27(4):1013–1026, 2016.

[28] Jean-Philippe Lessard, Jason D. Mireles James, and Christian Reinhardt. Computer assisted proof of transverse saddle-to-saddle connecting orbits for first order vector fields. *J. Dynam. Differential Equations*, 26(2):267–313, 2014.

[29] Rudolf J. Lohner. Computation of guaranteed enclosures for the solutions of ordinary initial and boundary value problems. In *Computational ordinary differential equations (London, 1989)*, volume 39 of *Inst. Math. Appl. Conf. Ser. New Ser.*, pages 425–435. Oxford Univ. Press, New York, 1992.

[30] J. D. Mireles James. Polynomial approximation of one parameter families of (un)stable manifolds with rigorous computer assisted error bounds. *Indag. Math. (N.S.)*, 26(1):225–265, 2015.

[31] J. D. Mireles James and Konstantin Mischaikow. Rigorous a posteriori computation of (un)stable manifolds and connecting orbits for analytic maps. *SIAM J. Appl. Dyn. Syst.*, 12(2):957–1006, 2013.

[32] J.D. Mireles James and Konstantin Mischaikow. Rigorous a-posteriori computation of (un)stable manifolds and connecting orbits for analytic maps. *SIAM J. Numer. Anal.*, 12(2):957–1006, 2013.

[33] Evelyn Sander and Thomas Wanner. Validated saddle-node bifurcations and applications to lattice dynamical systems. *SIAM J. Appl. Dyn. Syst.*, 15(3):1690–1733, 2016.

[34] Warwick Tucker. Validated numerics for pedestrians. In *European Congress of Mathematics*, pages 851–860. Eur. Math. Soc., Zürich, 2005.

[35] Warwick Tucker. *Validated numerics*. Princeton University Press, Princeton, NJ, 2011. A short introduction to rigorous computations.

[36] Jan Bouwe van den Berg and Jean-Philippe Lessard. Rigorous numerics in dynamics. *Notices Amer. Math. Soc.*, 62(9):1057–1061, 2015.

[37] Jan Bouwe van den Berg, Jean-Philippe Lessard, and Konstantin Mischaikow. Global smooth solution curves using rigorous branch following. *Math. Comp.*, 79(271):1565–1584, 2010.

[38] Thomas Wanner. Computer-assisted equilibrium validation for the dibolck copolymer model. *Discred and Continuous Dynamical Systems*, 37(2):1075–1107, 2017.

[39] Piotr Zgliczynski. C^1 Lohner algorithm. *Found. Comput. Math.*, 2(4):429–465, 2002.